Bell-shaped magnetic hollow porous carbon: an efficient and sustainably recycled iodine absorbent in aqueous

Chang Sun,[a] Dehui Yang,[a] Ye Li,[a] Yaxi Shu,[a] Huiyong Wang,[b] Guoqing Zhuang,*[c] Baozhan Zheng,*[a] Juan Du,*[a] and Yong Guo[a]

[a] *College of Chemistry, Sichuan University, Chengdu 610064, China*

[b] *School of Chemistry and Chemical Engineering, Henan Normal University, Xinxiang 453007, Henan, China*

[c] *Sichuan Academy of Forestry, Chengdu 610081, Sichuan, China*

**Corresponding authors: zgq@sclky.com (G.Z.); zhengbaozhan@scu.edu.cn (B.Z.); dujuanchem@scu.edu.cn (J.D.)*

Adsorption equations

Adsorption kinetics. The iodine adsorption kinetics of the H-PC were scrutinized using the pseudo-first-order kinetic model (Eq. S1), the pseudo-second-order kinetic model (Eq. S2), and the intra-particle diffusion model (Eq. S3). The adsorption parameters were calculated to examine the kinetic behavior of the adsorbed iodine:

$$\ln(q_e-q_t) = \ln q_e - k_1 t \tag{S1}$$

$$\frac{t}{q_t} = \frac{t}{q_e} + \frac{1}{k_2 q_e^2} \tag{S2}$$

$$q_t = k_i t^{\frac{1}{2}} + c \tag{S3}$$

Where q_e (mg/g) represented the equilibrium adsorption capacity, q_t (mg/g) denoted the adsorption amount at time t, t (min) signified the contact time and k_1 (min^{-1}) stood for the pseudo-first-order kinetic rate constant. Additionally, k_2 (g/mg·min) was the pseudo-second-order kinetic rate constant, and k_i ($mg/g \cdot min^{-1/2}$) indicated the internal diffusion rate constant of the particles.

Adsorption isotherms. Langmuir, Freundlich, and Dubinin-Radushkevich (D-R) adsorption isotherm were employed to analyze the adsorption data, and the relevant adsorption parameters were calculated. The linear expressions for these isotherms were outlined below:

$$\frac{C_e}{q_e} = \frac{C_e}{q_m} + \frac{1}{K_L q_m} \tag{S4}$$

$$\lg q_e = \lg K_F + \frac{\lg C_e}{n} \quad \text{(S5)}$$

$$\ln(q_e) = \ln(q_s) - \beta\varepsilon^2 \quad \text{(S6)}$$

Where C_e (mg/L) represented the equilibrium concentration of iodine, q_e (mg/g) signified the adsorption capacity at equilibrium, q_m (mg/g) indicated the maximum adsorption capacity corresponding to complete monolayer coverage, K_L (L/mg) represented the adsorption constant based on the Langmuir model, and K_F ((mg/g)(L/mg)$^{1/n}$) was the constant for adsorption based on the Freundlich model. Additionally, q_s (mg/g) stood for the theoretical isothermal saturation capacity, β (mol^2/kJ^2) was the D-R isotherm constant, ε was the Polanyi adsorption potential.

Adsorption thermodynamics. The adsorption experiments were conducted across a range of temperatures from 288.15K to 328.15K. The thermodynamic parameters, including the change in enthalpy (ΔH^0), change in free energy (ΔG^0), and change in entropy (ΔS^0), were calculated using Gibbs-Helmholtz and Van't Hoff equations, applying fundamental thermodynamic principles.

$$\ln(K_d) = -\frac{\Delta H^0}{RT} + \frac{\Delta S^0}{R} \quad \text{(S7)}$$

$$K_d = \frac{Q_e}{C_e} \quad \text{(S8)}$$

$$\Delta G^0 = -RT\ln(K_d) \quad \text{(S9)}$$

Where Q_e (mg/g) and C_e (mg/L) represented the adsorption capacity and concentration at equilibrium, respectively. K_d is the thermodynamic

equilibrium constant, R is the gas constant of 8.314 (J mol^{-1} K), and T (K) is the thermodynamic temperature. The values of ΔH^0 and ΔS^0 were determined from the intercept and slope of Fig. 4D.

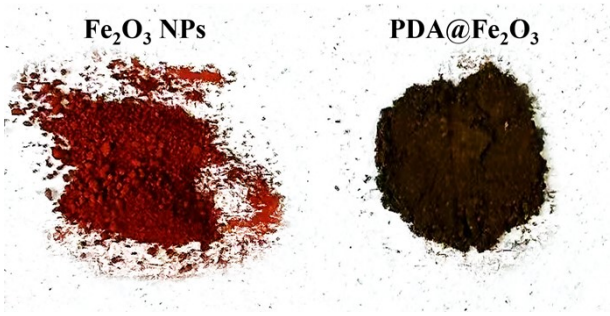

Fig. S1. The color of Fe_2O_3 and PDA@Fe_2O_3, respectively.

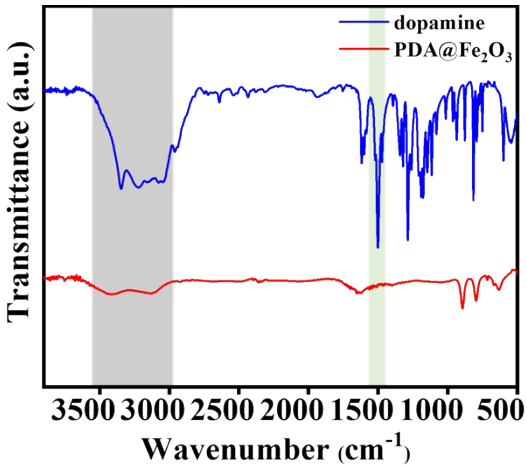

Fig. S2. FT-IR spectra of dopamine and PDA@Fe_2O_3.

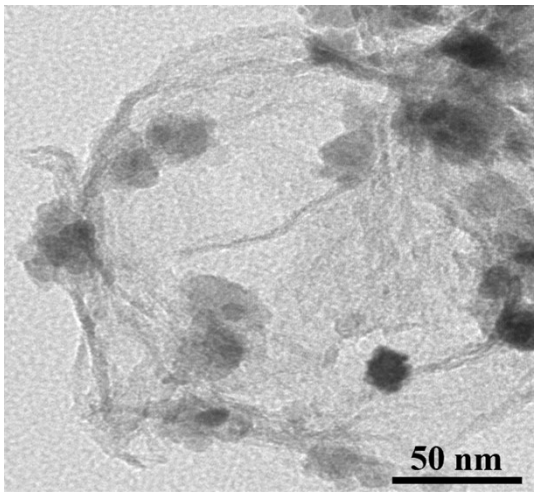

Fig. S3. The HRTEM image of BM-PC.

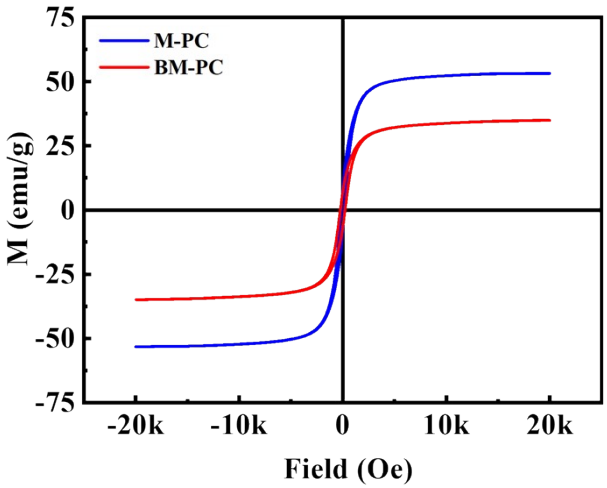

Fig. S4. The magnetization curves of M-PC and BM-PC.

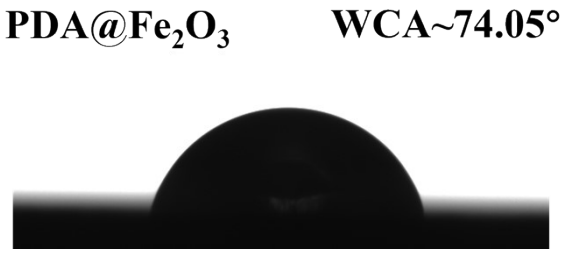

Fig. S5. The water contact angle of PDA@Fe_2O_3.

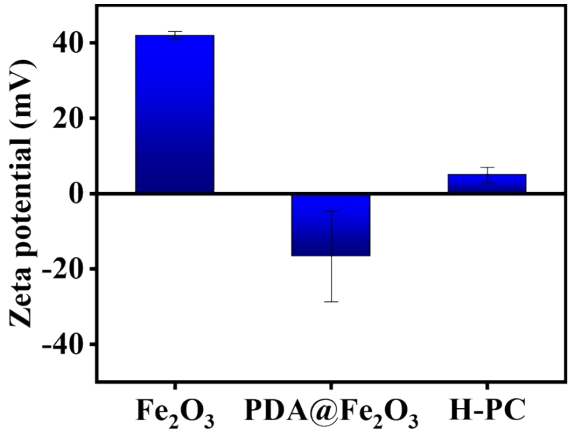

Fig. S6. The zeta potentials of Fe_2O_3, PDA@Fe_2O_3, and H-PC, respectively.

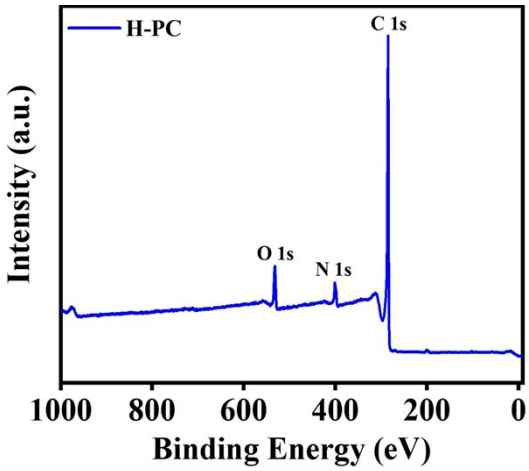

Fig. S7. XPS survey spectrum of H-PC.

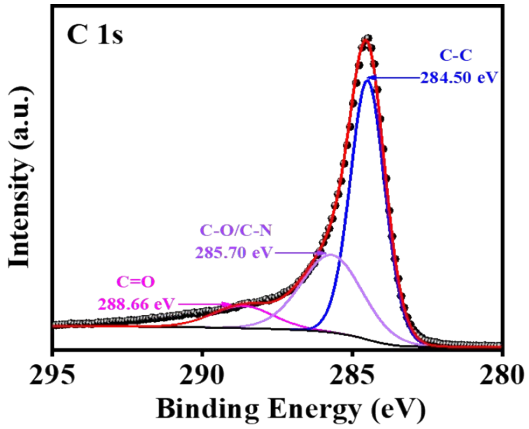

Fig. S8. High-resolution XPS spectrum of C 1s for H-PC.

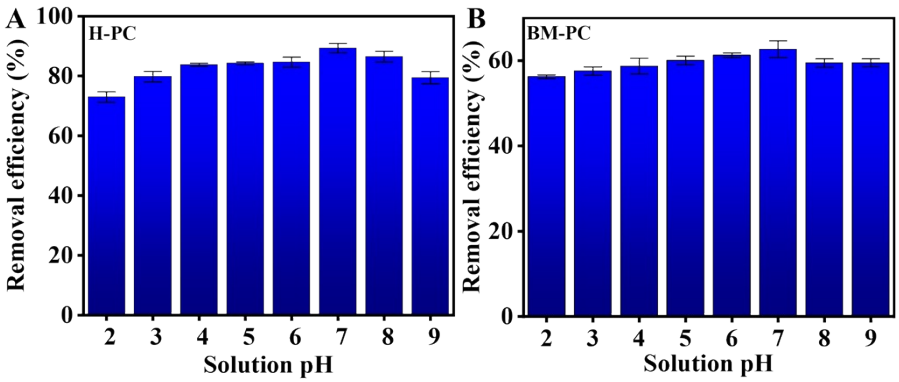

Fig. S9. The effects of pH on iodine adsorption by H-PC (A), BM-PC (B). Experimental conditions: $[I_3^-]$ = 1500 mg/L, pH = 2~9, T = 25 ℃. Error bars represent standard deviation of triplicate measurements.

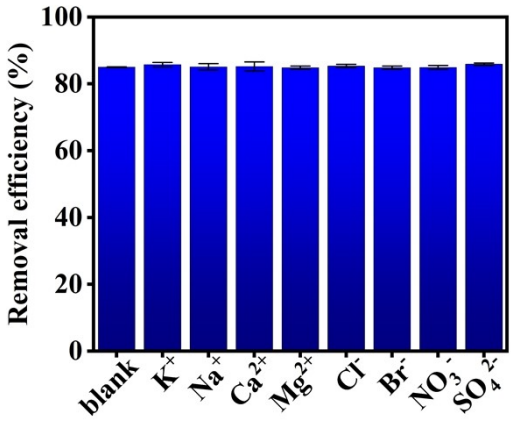

Fig. S10. Effects of coexisting ions on iodine adsorption by H-PC. Experimental conditions: $[I_3^-]$ = 1500 mg/L, [H-PC] = 0.3 g/L, pH = 7, T = 25 ℃. Error bars represent standard deviation of triplicate measurements.

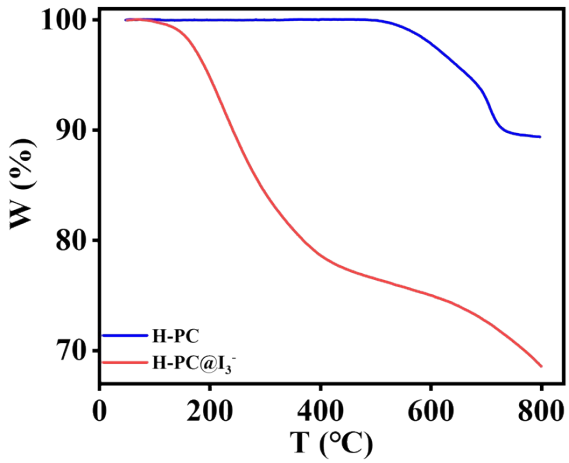

Fig. S11. TGA curves of H-PC before and after the adsorption of iodine (H-PC@I_3^-).

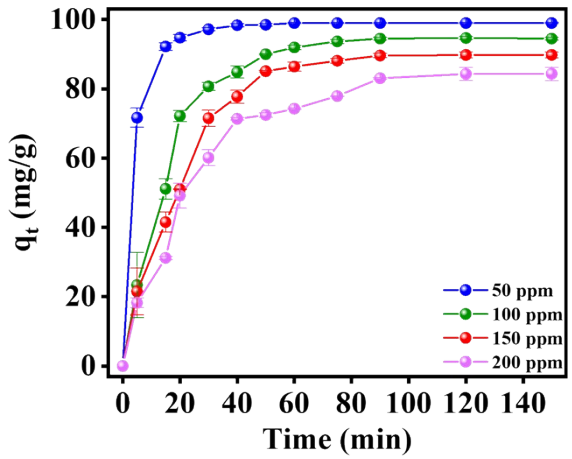

Fig. S12. Adsorption of iodine on H-PC adsorbents as a function of time. Experimental conditions: [I_3^-] = 50~200 mg/L, [H-PC] = 0.3 g/L, pH = 7, T = 25 °C. Error bars represent standard deviation of triplicate measurements.

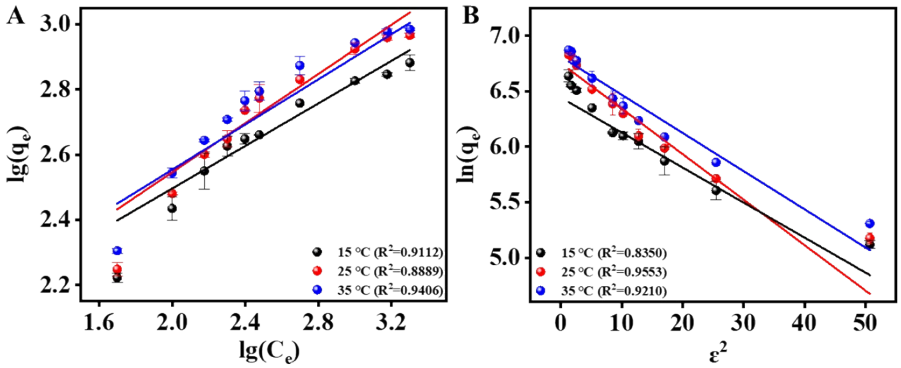

Fig. S13. Corresponding fitted data by Freundlich (A) and D-R isotherm models (B). Experimental conditions: [I_3^-] = 1500 mg/L, [H-PC] = 0.3 g/L, pH = 7, T = 15~35 ℃. Error bars represent standard deviation of triplicate measurements.

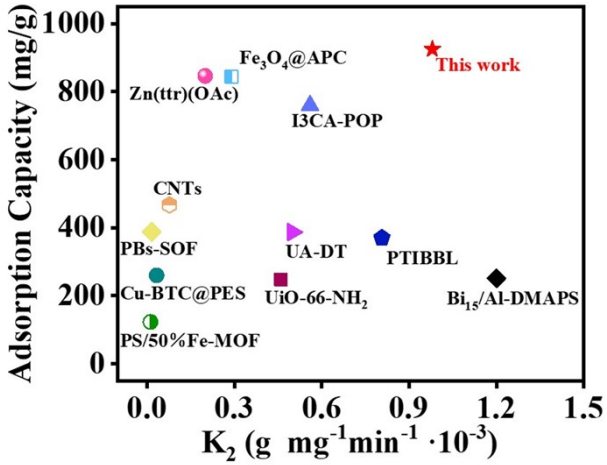

Fig. S14. Iodine adsorption capacity and pseudo-second-order kinetic adsorption rate constant of different absorbents.

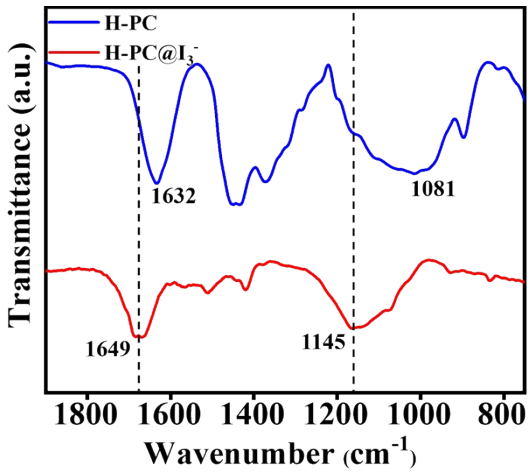

Fig. S15. The FT-IR spectra of H-PC before and after the adsorption of iodine (H-PC@I_3^-).

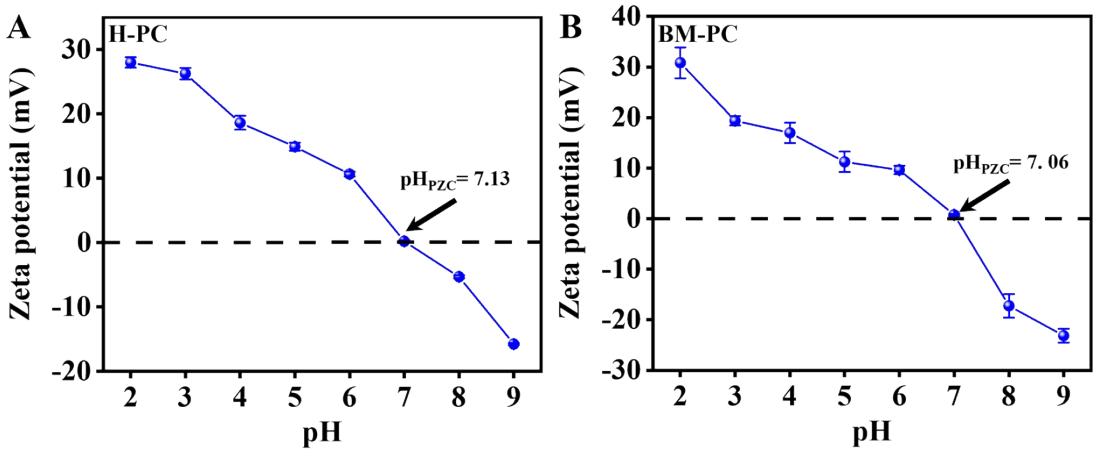

Fig. S16. Zeta potentials of H-PC (A) and BM-PC (B) at different pHs.

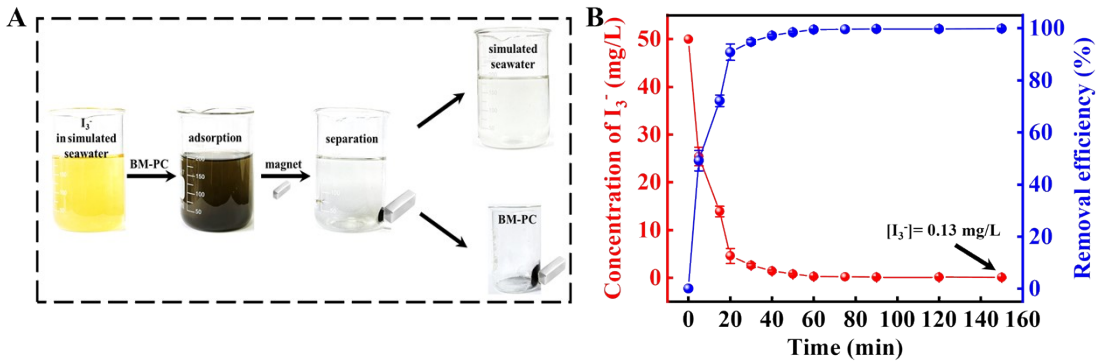

Fig. S17. Application of BM-PC in simulated seawater: (A) schematic diagram of the process, (B) adsorption of iodine on BM-PC adsorbents as a function of time. Experimental conditions: $[I_3^-]$ = 50 mg/L, [BM-PC] = 5 g/L, pH = 7, T = 25 ℃. Error bars represent standard deviation of triplicate measurements.

Table S1. Kinetics parameters of iodine adsorption on H-PC and PC. Experimental conditions: [I_3^-] = 1500 mg/L, [H-PC] = 0.3 g/L, pH = 7, T = 25 ℃.

Equations	Parameters	H-PC	PC
	$q_{e(exp)}$ (mg/g)	945.97	318.27
Pseudo-first-order	$q_{e(cal)}$ (mg/g)	639.33	205.81
	k_1 (min^{-1})	0.03	0.03
	R^2	0.9751	0.8777
Pseudo-second-order	$q_{e(cal)}$ (mg/g)	1016.53	344.82
	k_2 ($g \cdot mg^{-1}\ min^{-1}$)	$9.8*10^{-4}$	2.9 E-05
	R^2	0.9987	0.9974

Table S2. Parameters for Langmuir, Freundlich and D-R models of iodine adsorption on H-PC. Experimental conditions: $[I_3^-]$ = 50~1500 mg/L, [H-PC] = 0.3 g/L, pH = 7, T = 15~25 ℃.

Equations	Parameters	Temperature		
		15 ℃	25 ℃	35 ℃
	$q_{m(exp)}$ (mg/g)	809.32	939.22	973.93
Langmuir isotherm	$q_{m(cal)}$ (mg/g)	819.67	927.00	971.10
	K_L (L/mg)	0.0045	0.0047	0.0050
	R^2	0.9955	0.9993	0.9996
Freundlich isotherm	K_F ((mg/g)(L/mg)$^{1/n}$)	44.49	47.77	54.65
	n	2.5553	2.4213	2.4902
	R^2	0.9392	0.9199	0.9220
D-R isotherm	β	0.0327	0.0341	0.0320
	q_s (mg/g)	653.93	822.72	868.66
	E (kJ/mol)	3.9103	3.8192	3.9528
	R^2	0.9155	0.9368	0.9348

Table S3. Thermodynamic parameters for the adsorption of iodine on H-PC at 200 and 300 mg/L. Experimental conditions: $[I_3^-]$ = 200~300 mg/L, [H-PC] = 0.3 g/L, pH = 7, T = 15~55 ℃.

Initial concentration of iodine	T (K)	ΔH^0 (kJ mol^{-1})	ΔS^0 (J mol^{-1} K^{-1})	ΔG^0 (kJ mol^{-1})
200 ppm	288.15	14.80	61.70	-2.80
	298.15			-3.60
	308.15			-4.19
	318.15			-4.91
	328.15			-5.61
300 ppm	288.15	15.85	61.54	-1.88
	298.15			-2.48
	308.15			-3.10
	318.15			-3.79
	328.15			-4.31

Table S4. Comparative evaluation of iodine adsorption by H-PC and other adsorbents.

Adsorbent	Adsorption capacity (mg/g)	k_2 (g/mg·min)	Equilibrium time (mins)	Reference
H-PC	945.97	9.8×10^{-4}	60	This work
PC	318.27	2.9×10^{-5}	60	This work
n-CF@OCDs	190.10	—	20	1
Fe_3O_4@APC	844.60	2.9×10^{-4}	90	2
Cu-BTC@ PES	260.28	3.3×10^{-5}	480	3
PS/50 %Fe-MOF	123.00	1.2×10^{-5}	—	4
CNTs	467.38	7.7×10^{-5}	420	5
UiO-66-NH_2	248.05	4.6×10^{-4}	—	6
PBs-SOF	388.39	1.6×10^{-5}	30	7
UA-DT	387.59	5.0×10^{-4}	—	8
PTIBBL	370.74	8.1×10^{-4}	390	9
Bi_{15}/Al-DMAPS	215.70	1.2×10^{-3}	—	10
I3CA-POP	760.00	5.6×10^{-4}	30	11
Zn(ttr)(OAc)	846.11	2.0×10^{-4}	660	12
PHCP-4	416.67	3.5×10^{-3}	120	13
HCPs-TBP	235.85	2.4×10^{-4}	—	14

Reference

[1] B. Zheng, X. Liu, J. Hu, F. Wang, X. Hu, Y. Zhu, X. Lv, J. Du and D. Xiao, *J. Hazard. Mater.*, 2019, **368**, 81-89.

[2] H.E. Emam, M. El-Shahat and R.M. Abdelhameed, *Ind. Crop. Prod.*, 2023, **193**, 116201.

[3] Q. Zhao, L. Zhu, G. Lin, G. Chen, B. Liu, L. Zhang, T. Duan and J. Lei, *ACS Appl. Mater. Interfaces*, 2019, **11**, 42635-42645.

[4] S. Nikpour, Z. Ansari-Asl and T. Sedaghat, *Inorg. Chem. Commun.*, 2022, **136**, 109141.

[5] C. Zhao, L. Ge, R. Wang, H. Chu, L. Mai, W. Zha, Y. Wang and C. Xu, *Fuel*, 2023, **352**, 129061.

[6] S. Tian, Z. Yi, J. Chen and S. Fu, *J. Hazard. Mater.*, 2023, **443**, 130236.

[7] Z. Xu, P. Zhang, W. Teng, M. He, S. Liu, K. Li and H. Wang, *J. Environ. Chem. Eng.*, 2023, **11**, 110139.

[8] Z. Shi, X. Huang, Y. Zhao, J. Li, Y.Q. Tian, P.P. Zhang, M. Zhu and M. Zhao, *Environ. Res.*, 2023, **235**, 116617.

[9] M. Huang, L. Yang, X. Li and G. Chang, *Chem. Commun.*, 2020, **56**, 1401-1404.

[10] M. Alsalbokh, N. Fakeri, A.A. Rownaghi, D. Ludlow and F. Rezaei, *Chem. Eng. J.*, 2021, **409**, 128277.

[11] J. Yu, L. Song, Y. Wang, T. Bai, C. Long, M. Wu, Y. Feng and J. Mi, *J. Radioanal. Nucl. Chem.*, 2023, **332**, 4271-4290.

[12] J. Qin, W. Zhang, Y. Chen, R. Liu and Y. Fan, *Environ. Sci. Pollut. Res.*, 2021, **28**, 28797-28807.
[13] J. Ma, Z. Shi, T. Wang, X. Huang, Y. Zhao, J. Wang, J. Li, D. Wang, L. Sun, G. Dong and M. Zhao, *ACS Sustain. Chem. Eng.*, 2024, **12**, 12113-12125.
[14] J. Bi, K. Bao, M. Zhao, Y. Zha, T. Chen, C. Huang and Z. Lv, *Appl. Surf. Sci*., 2025, **688**, 162385.